

Article

Benchmark Study on Phosphorescence Energies of Anthraquinone Compounds: Comparison between TDDFT and UDFT

Yujie Guo, Lingyu Zhang and Zexing Qu * 

Institute of Theoretical Chemistry, College of Chemistry, Jilin University, Changchun 130021, China

* Correspondence: zxqu@jlu.edu.cn

Abstract: Phosphorescent material is widely used in light-emitting devices and in the monitoring of cell phenomena. Anthraquinone compounds (AQs), as important phosphorescent materials, have potential applications as emitters for highly efficient organic light-emitting diodes (OLEDs). Therefore, the accurate calculation of the phosphorescence energy of anthraquinone compounds is particularly important. This study mainly analyzes the phosphorescence energy calculation method of anthraquinone compounds. The time-dependent density functional theory (TDDFT) and the unrestricted density functional theory (UDFT) with seven functionals are selected to calculate the phosphorescence of AQs, taking the high-precision coupled-cluster singles and doubles (CC2) method as a reference. The results showed that the mean unsigned error (MUE) of UDFT was 0.14 eV, which was much smaller than that of TDDFT at 0.29 eV. Therefore, UDFT was more suitable for calculating the phosphorescence energy of AQs. The results obtained by different functionals indicate that the minimum MUE obtained by M06-2X was 0.14 eV. More importantly, the diffuse function in the basis set played an important role in calculating the phosphorescence energy in the M06-HF functional. In the BDBT, FBDBT, and BrBDBT, when M06-HF selected the basis set containing a diffuse function, the differences with CC2 was 0.02 eV, which is much smaller than the one obtained without a diffuse function at 0.80 eV. These findings might be of great significance for the future study of the phosphorescence energy of organic molecules.

Keywords: phosphorescence energies; time-dependent density functional theory (TDDFT); anthraquinone



Citation: Guo, Y.; Zhang, L.; Qu, Z. Benchmark Study on Phosphorescence Energies of Anthraquinone Compounds: Comparison between TDDFT and UDFT. *Molecules* **2023**, *28*, 3257. <https://doi.org/10.3390/molecules28073257>

Academic Editor: Athanassios C. Tsipis

Received: 3 March 2023

Revised: 4 April 2023

Accepted: 4 April 2023

Published: 5 April 2023



Copyright: © 2023 by the authors. Licensee MDPI, Basel, Switzerland. This article is an open access article distributed under the terms and conditions of the Creative Commons Attribution (CC BY) license (<https://creativecommons.org/licenses/by/4.0/>).

1. Introduction

Purely organic phosphorescence emitting molecules have attracted tremendous attention in the past few decades due to their advantages of great variety, low price, and ease of fabrication [1–4]. In general, phosphorescent materials need an efficient intersystem crossing (ISC) rate, and the metal-free molecules, which usually have a small spin–orbit coupling (SOC), struggle to emit phosphorescence [5–10]. However, El-Sayed’s rule states that the ISC rate could be relatively large if the radiationless transition involves a change in molecular orbital type (for example, from a (π , π^*) singlet state to a (n , π^*) triplet state and vice versa [11]). This rule is very useful in designing purely organic phosphorescence molecules. Recently, it has been suggested that anthraquinone compounds (AQs) have a fast ISC rate and can be used as the important components for metal-free phosphorescent materials [12,13]. The diversity of the electronic structure of Aqs has drawn more interest regarding research and development space in the fields of photochemistry. As a result, the detailed information on the low-lying excited states, as well as the phosphorescence emission of AQs, has become a popular issue in theoretical research [14,15].

The phosphorescence emission usually refers to the radiation transition from the lowest triplet excited state (T_1) to the singlet ground state (S_0), and the calculation of the triplet excited state is of particular importance in the simulation of the phosphorescence spectrum. The triplet excited states usually show the opposite electronic behavior when compared to the ground state, and the dynamic correlation should be included in the

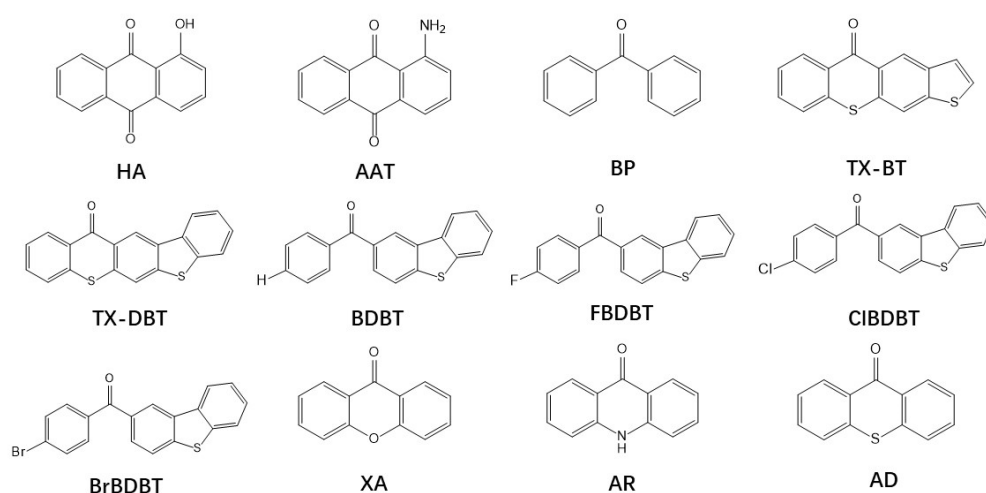
calculation of the triplet excited states. Thus, the coupled-cluster method, as a high level ab initio method that includes dynamic correlation, is usually adopted for the calculation of phosphorescence energy. Thiel and colleagues [16,17] tested singlet–triplet energy gaps for small organic molecules (limited to 15 atoms) with coupled cluster methods (CC3 [18] and CCSDR [19]). Although further calculations with complete active space with the second-order perturbation theory (CASPT2) [20,21] and coupled-cluster singles and doubles CC2 [22] can be extended to 40 atoms [23–29], these methods cannot overcome the “Index Wall” of high-level wave function theory (WFT). Density functional theory (DFT) [30–32] can obtain the energy and density of molecules in a way that is easy to calculate and DFT provides a balance between accuracy and computational cost for ground state calculations. Time-dependent density functional theory (TDDFT) [33–37] is the most widely used tool for calculating not only excitation energies, but also excited state properties, such as dipole moments and the emission spectrum, which is conducted with a computational cost between semiempirical methods and wave function theory. Latouche and colleagues benchmarked the phosphorescence spectra of transition metal complexes containing platinum and iridium with the unrestricted density functional theory (UDFT), time-dependent density functional theory (TDDFT), and the Tamm–Dancoff approximation (TDA) [38–45] methods. The results showed that UDFT and TDA performed better than TDDFT [46]. Recently, Ehara and colleagues used the symmetry-adapted cluster-configuration interaction (SAC-CI) [47] method and TDDFT to benchmark the geometric structures and phosphorescence energy of heterocyclic compounds; they concluded that both methods could provide accurate results in calculating phosphorescence energies of purely organic molecules [48]. Each of these methods has its advantages and limitations.

In the UDFT calculations, the singlet ground state and triplet excited state were optimized separately and could be easily converted for both states. However, in this approach, the Kohn–Sham orbitals were optimized and restricted to a different state; further, the phosphorescence energy was obtained at different levels. More importantly, the spin contamination of the triplet state from the unrestricted treatment usually underestimates the phosphorescence energy. On the other hand, the TDDFT treatment was free of spin contamination, and the triplet excited state and the singlet ground state can be calculated at the same level. However, the shortcoming of TDDFT is that the Rydberg states, which are caused by the Rydberg excitations, could increase the difficulty of the convergence for the triplet states [49,50]. Thus, the UDFT treatment, which has no Rydberg excitation, could be easier to converge for the optimization of the triplet state [51,52]. Since the accuracy for all kinds of DFT calculations is also dependent on the choice of the functional, this work also investigates the functional and basis set effects on the calculation of phosphorescence energies with DFT. At the same time, in order to better calculate the phosphorescence energy and to determine the characteristics of the electron excitation, the charge transfer characteristics and the stabilization energy were calculated using the natural bond orbital (NBO) [53–55].

2. Computational Details

A series of 12 typical experimentally synthesized anthraquinone compounds and AQs, including 1-hydroxyanthraquinone (HA); aminoanthraquinone (AAT); benzophenone (BP); 5H-thieno[3,2-b] thioxanthen-5-one (TX-BT); 13H-benzo[4,5] thieno[3,2-b]thioxanthen-13-one (TX-DBT); dibenzo[b,d]thiophen-2-yl (phenyl)methanone (BDBT); ben-zo [b,d]thiophen-2-yl (4-fluorophenyl) methanone (FBDBT); (4-chlorophenyl) (dibenzo[b,d]thiophen-2-yl) methanone (ClBDBT); (4-bromophenyl) (dibenzo[b,d] thiophen-2-yl)methanone (ClBDBT); (4-bromophenyl) (dibenzo[b,d]thiophen-2-yl) methanone (BrBDBT); xanth-9-one (XA); 10H-acridin-9-one (AR); and thioxanthone (AD) [56–63]—as is shown in Scheme 1—were used to calculate the phosphorescence energies. Here, the HA, XA, AR, and AD molecules were constrained to a C_s symmetry and the other molecules were in a C_1 symmetry. For the molecules with C_1 symmetry, the natural transition orbital (NTO) and the frontier orbital analyses were used to determine the wave functions of the lowest triplet excited state.

Seven typical functionals of PEB, PBE0 [64], B3LYP [65], CAM-B3LYP [66], ω B97XD [67], M06-2X [68], and M06-HF [69,70]—ranging from GGA to meta-GGA functionals and cc-pVTZ—were used for the DFT calculations. In this work, TDDFT and UDFT were used to optimize the geometry and to compute the energy for the lowest triplet excited state, and thus the combination of the above two methods can yield the following groups of calculation schemes. If the geometries were optimized by UDFT and the excitation energies were computed with TDDFT, based on UDFT optimized geometries, then we denote this scheme as TD//UDFT. On the other hand, if both the optimized geometries and excitation energies were computed with UDFT, we denote this scheme as U//UDFT. In addition, there are other two kinds of schemes that were characterized as TD//TDDFT and U//TDDFT, in which the geometries were optimized by TDDFT and the excitation energies were computed with TDDFT and UDFT, respectively. The schemes are compared in Tables S18 and S19, and the results for TD//TDDFT and U//TDDFT were similar. All the geometry optimizations and single-point calculations with DFT were computed using Gaussian16 software [71]. The charge transfer characteristics and the stabilization energies were obtained using NBO Version 3.1 in Gaussian16 software. Besides DFT, the coupled-cluster method CC2 was used as the benchmark for calculation of the phosphorescence energies. In addition, all the CC2 results were obtained from the MOLPRO2021 package [72,73].



Scheme 1. Twelve anthraquinone compounds (AQs).

3. Results

3.1. Geometry Optimization

In this work, we calculated the phosphorescence energy; furthermore, the triplet state could be optimized by means of TDDFT and UDFT. On this basis, the root mean square deviation (RMSD) of the two geometries was calculated to measure the geometric deviation between them. Here, we aligned two geometries by visual molecular dynamics (VMD) [74], which was equivalent to minimizing the RMSD between the two geometries by translating and rotating one geometry.

$$\text{RMSD} = \sqrt{\frac{1}{N} \sum_i [(x_i - x'_i)^2 + (y_i - y'_i)^2 + (z_i - z'_i)^2]}$$

As shown in Table 1, based on the RMSD values, the average value of the 12 systems is 0.03 Å. This indicates that the geometry optimized by TDDFT and UDFT is very similar. Here, it should be noted that TDDFT suffers from a Rydberg state for HA, XA, AR, and AD, which caused problems in the optimization and electronic state selection, which was not easy to converge. In the optimization of TDDFT, we needed to choose the right state to track in order to obtain a reasonable geometry, not the lowest triplet state. UDFT is not affected

by the Rydberg state during geometry optimization and was a more suitable method for optimization than TDDFT. The calculated phosphorescence energy values further show that the geometries obtained by TDDFT and UDFT optimization have little effect on phosphorescence energy calculation. As shown in Table 2 and Table S18, the difference in the mean unsigned error (MUE) for phosphorescence energy was about 0.01 eV, further proving that the geometries obtained by TDDFT and UDFT had little influence on the calculation of the phosphorescence energy. Therefore, it could be concluded that the UDFT method was more suitable for the geometry optimization of phosphorescence energy.

Table 1. The root mean square deviation (RMSD) in Å of the two AQs geometries that were optimized by TDDFT and UDFT, respectively.

Molecular	RMSD	Molecular	RMSD
HA	0.00	FBDBT	0.02
AAT	0.05	CIBDBT	0.03
BP	0.01	BrBDBT	0.03
TX-BT	0.14	XA	0.03
TX-DBT	0.01	AR	0.02
BDBT	0.02	AD	0.01

The average RMSD for the AQs is 0.03 Å.

Table 2. The energy differences ΔE (in eV) relative to CC2 for the phosphorescence energy of AQs were calculated by TD//UDFT with different functionals (PBE, PBE0, B3LYP, CAM-B3LYP, ω B97XD, M06-2X, and M06-HF) at the cc-pVTZ level.

	CC2	PBE	PBE0	B3LYP	CAM-B3LYP	ω B97XD	M06-2X	M06-HF
HA	2.55	−0.87 *	−0.80	−0.75	−0.68	−0.57	−0.41	−0.25 *
AAT	2.03	−0.75	−0.67	−0.64	−0.53	−0.46	−0.33	−0.11
BP	2.50	−0.62	−0.39	−0.34	−0.27	−0.18	−0.11	−0.26
TX-BT	2.67	−0.49	−0.71	−0.59	−0.83	−0.68	−0.28	−0.14
TX-DBT	2.91	−0.77	−0.58	−0.57	−0.47	−0.39	−0.36	−0.32
BDBT	2.52	−0.65	−0.42	−0.37	−0.30	−0.21	−0.13	−0.25
FBDBT	2.56	−0.65	−0.44	−0.39	−0.33	−0.23	−0.15	−0.27
CIBDBT	2.52	−0.66	−0.43	−0.39	−0.31	−0.22	−0.14	−0.26
BrBDBT	2.51	−0.66	−0.43	−0.38	−0.31	−0.21	−0.14	−0.25
XA	3.16	−0.68 *	−0.76	−0.68 *	−0.71	−0.60	−0.55	−0.59
AR	2.83	−0.65 *	−0.63	−0.59	−0.54	−0.47	−0.48	−0.53
AD	2.93	−0.71 *	−0.64	−0.60	−0.56	−0.48	−0.44	−0.44
MUE ^(a)	—	0.68	0.57	0.53	0.49	0.39	0.29	0.31

^(a) MUE is the mean unsigned error between the calculated phosphorescence energy and CC2. * The symmetry of the lowest triplet excited state (T_1) is different from that of the ground states, so the second triplet excited state (T_2) is selected to obtain ΔE .

3.2. Phosphorescence Energy

Tables 2 and 3 show the triplet state geometry optimization by means of UDFT, and the phosphorescence energy was calculated by using TDDFT and UDFT, respectively. Compared with TDDFT, although the electronic states of UDFT were unreasonable, the lowest triplet excited state energy calculated by TDDFT was too low, making UDFT more suitable for calculating the phosphorescence energy. In most cases, UDFT is recommended to calculate the lowest triple excited state, whether it is a single point calculation or a geometric optimization. Although the spin contamination existed in the UDFT, it can be seen that the S^2 values for the triplet states of AQs are around 2.0 for all of the functionals (as shown in Table S22). Thus, the effect of spin contamination on the results is small.

Furthermore, it could be concluded that the phosphorescence energy obtained by TDDFT was underestimated and all the values were lower than those found in CC2. As the calculation of DFT was affected by the functional, the analysis of different functionals

showed that PBE without the Hartree–Fock exchange provided the worst results, with an MUE of 0.68 eV. When the Hartree–Fock exchange was introduced into the functional, the MUE decreased from 0.68 eV to 0.39 eV. The MUE of PBE0, B3LYP, CAM-B3LYP, and ω B97XD were 0.57 eV, 0.53 eV, 0.49 eV and 0.39 eV, respectively. It is shown that the introduction of the Hartree–Fock exchange was helpful to reduce the effect of TDDFT on the underestimation of phosphorescence energy, and also in bringing the calculated phosphorescence energy to be closer to CC2. The MUE of the high-precision M06-2X and M06-HF was 0.29 eV and 0.31 eV, respectively. In addition, the M06-2X was functional with the closest accuracy to CC2. Therefore, the functional of the M06 series was more suitable for calculating phosphorescence energy.

The data in Table 3 show that the phosphorescence energy values were calculated by a U//UDFT fluctuate around the CC2 values. The closest to CC2 was M06-2X with an MUE of 0.14 eV, followed by ω B97XD with an 0.18 eV. With the increase in the Hartree–Fock exchange in the different functionals, the MUE values decreased from 0.66 eV to 0.18 eV. We find that increasing the percentage of the Hartree–Fock exchange significantly increased the accuracy of the functional. At this time, the MUE of ω B97XD was 0.18 eV, and ω B97XD was similar to that of the M06 series. The lowest MUE value of M06-2X was 0.14 eV, while the MUE value of M06-HF was 0.24 eV. The reason for this phenomenon was that M06-HF cannot calculate the three systems of BDBT, FBDBT, and BrBDBT well. Table S20 shows the result of removing the BDBT, FBDBT, and BrBDBT. At this time, the MUE of M06-HF was reduced from 0.24 eV to 0.06 eV. The MUE of M06-HF became the minimum. When M06-HF was selected as the functional, the accuracy could be improved by adding the diffuse function in a basis set, such as aug-cc-pVDZ. In Figure 1, we can see that M06-HF could achieve an ideal accuracy under the U//UDFT scheme after adding the diffuse function in the basis sets. In Table 3, we also compared the computed results to the experimental values. Generally speaking, the MUEs were relative to CC2 and the experimental values show similar trends. By using experimental values as a reference, the MUEs of PBE, PBE0, B3LYP, and CAM-B3LYP were 0.56 eV, 0.25 eV, 0.23 eV, and 0.22 eV, respectively—which were smaller than the ones that were achieved by using the CC2 as a reference. The MUEs of M06-2X and M06-HF were 0.24 eV and 0.46 eV, respectively, which are relative to the experimental values. The larger values of the MUE of M06-HF might come from the BDBT, FBDBT, and BrBDBT, as is shown in Table S16.

Table 3. The energy differences ΔE (in eV) relative to the CC2 for the phosphorescence energy of AQs, as calculated by U//UDFT with the different functionals (PBE, PBE0, B3LYP, CAM–B3LYP, ω B97XD, M06-2X, and M06-HF) at the cc-pVTZ level.

	PBE	PBE0	B3LYP	CAM-B3LYP	ω B97XD	M06-2X	M06-HF
HA	1.47	−0.49	−0.47	−0.36	−0.31	−0.23	−0.09
AAT	−0.40	−0.41	−0.38	−0.34	−0.3	−0.24	−0.17
BP	−0.24	−0.28	−0.18	−0.15	−0.11	−0.05	−0.02
TX–BT	−0.35	−0.34	−0.32	−0.30	−0.23	−0.07	0.14
TX-DBT	−0.62	−0.42	−0.44	−0.21	−0.14	−0.12	0.06
BDBT	−0.37	−0.28	−0.22	−0.14	−0.10	−0.03	0.75
FBDBT	−0.39	−0.29	−0.23	−0.15	−0.11	−0.04	0.75
CIBDBT	−0.39	−0.29	−0.23	−0.15	−0.10	−0.03	0.00
BrBDBT	−0.39	−0.29	−0.23	−0.15	−0.10	−0.03	0.78
XA	−0.59	−0.65	−0.53	−0.28	−0.23	−0.47	0.01
AR	1.19	−0.32	−0.44	−0.26	−0.20	−0.16	0.04
AD	1.50	−0.45	−0.45	−0.27	−0.20	−0.17	−0.02
MUE ^(a)	0.66	0.37	0.34	0.23	0.18	0.14	0.24
MUE ^(b)	0.56	0.25	0.23	0.22	0.21	0.25	0.46

^(a) MUE is the mean unsigned error between the calculated phosphorescence energy and the CC2. ^(b) MUE is the mean unsigned error between the calculated phosphorescence energy and the experimental value. The experimental values are shown in references [56–63].

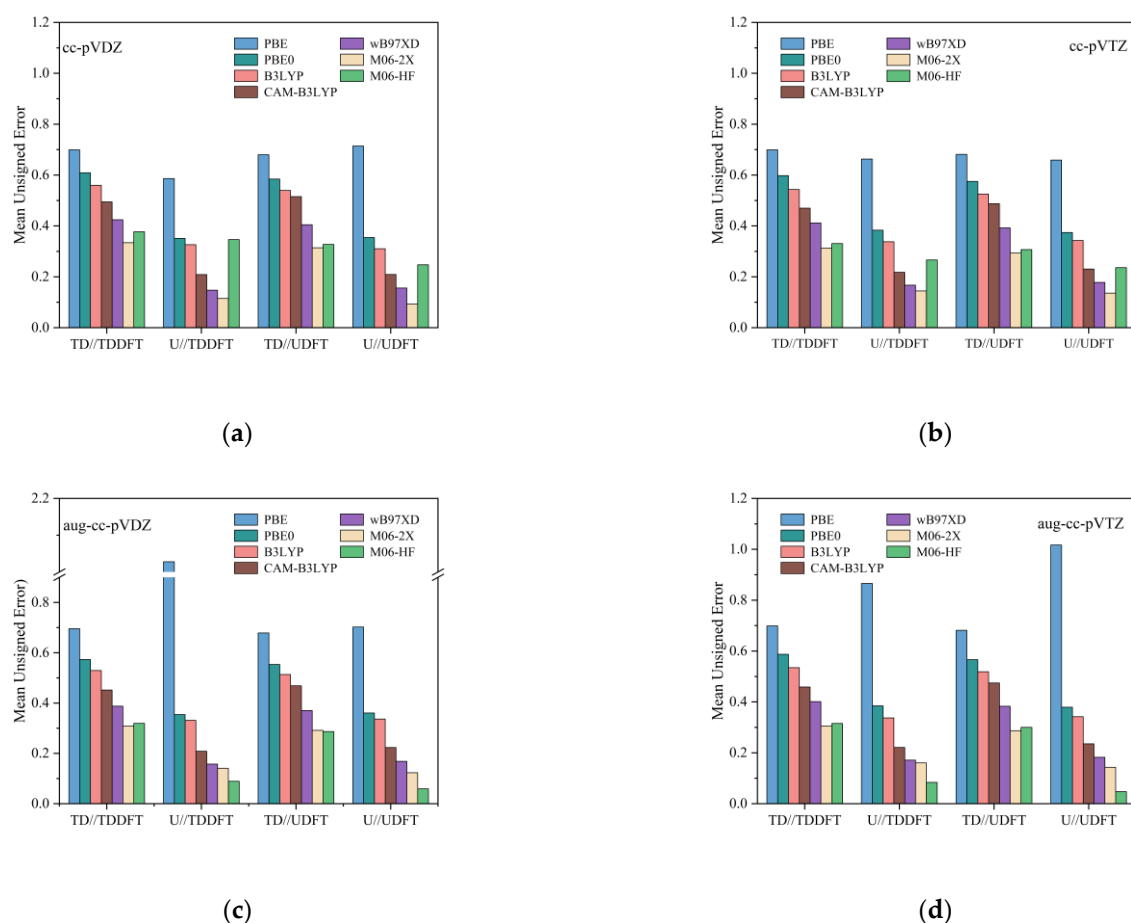


Figure 1. The MUE values obtained by different basis sets under the same phosphorescence energy calculation method and functionals. (a–d) represent the results obtained with the basis set of cc-pVDZ, cc-pVTZ, aug-cc-pVDZ, and aug-cc-pVTZ, respectively.

3.3. Basis Sets Effect

Figure 1 shows the results obtained by four different basis sets and shows that the MUE values obtained by the PBE functional without the Hartree–Fock exchange was 0.7 eV . In addition, it was noted that the MUE becomes gradually smaller as the Hartree–Fock exchange increases from 0.6 eV to 0.18 eV . The results obtained using range-separated functionals were close to the best-performing M06 series. Furthermore, the difference between the ωB97XD and M06-2X was within 0.05 eV . The results from cc-pVDZ and cc-pVTZ were consistent. The MUE ranged from 0.7 eV to 0.15 eV , but the MUE of M06-HF rose to 0.25 eV . When the diffuse function was added to the basis set, the MUE of M06-HF decreased significantly from 0.25 eV to 0.05 eV , which thus became the most accurate functional. M06-HF was sensitive to the basis set, and the inclusion of the diffuse function in the basis set had a significant impact on the accuracy of the phosphorescence energy. As shown in Figure 2, we calculated the functional of M06-HF and found that the main error came from the BDBT, FBDBT, and BrBDBT in the basis set without the diffuse function.

In the M06-HF calculation with the cc-pVDZ and cc-pVTZ basis set, the errors mainly came from the BDBT, FBDBT, and BrBDBT. Table S21 shows that for the BDBT, FBDBT, and BrBDBT molecules, when using a basis set without the diffuse function, the phosphorescence energy difference between M06-HF and CC2 was over 0.8 eV . However, by adding the diffuse function to the basis set, it was reduced to 0.02 eV . As shown in Table 4 and Figure 3, we analyzed the orbitals and charge transfer. It was found that the orbitals and charge transfer that were obtained using the basis set with a diffuse function were the same

as those of CIBDBT, while the orbitals of the other three systems were different, thereby leading to their large errors.

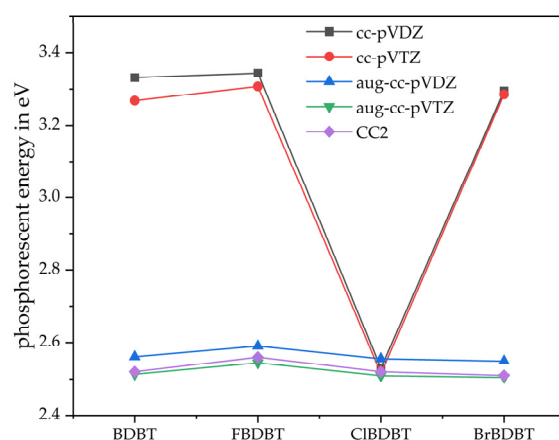


Figure 2. A comparison of the results of the BDBT, FBDBT, CIBDBT, and BrBDBT using four basis cc-pVDZ, cc-pVTZ, aug-cc-pVDZ, aug-cc-pVTZ and CC2.

Table 4. The NBO analysis of the charge transfer and stabilization energy, E (2), of the AQs at the M06-HF/cc-pVTZ and M06-HF/aug-cc-pVTZ level.

cc-pVTZ		aug-cc-pVTZ	
Charge Transfer	E (2) kcal/mol	Charge Transfer	E (2) kcal/mol
HA	σ^* (C7-C10) \rightarrow σ^* (C3-C4)	σ^* (C7-C10) \rightarrow σ^* (C3-C4)	176.24
AAT	σ^* (C8-C9) \rightarrow σ^* (C7-C10)	σ^* (C8-C9) \rightarrow σ^* (C7-C10)	105.28
BP	σ^* (C19-C21) \rightarrow σ^* (C15-C17)	σ^* (C19-C21) \rightarrow σ^* (C15-C17)	271.00
TX-BT	σ^* (C3-C4) \rightarrow σ^* (C5-C6)	σ^* (C3-C4) \rightarrow σ^* (C5-C6)	180.49
TX-DBT	σ^* (C3-C4) \rightarrow σ^* (C7-C8)	σ^* (C3-C4) \rightarrow σ^* (C7-C8)	249.08
BDBT	σ^* (C14-C15) \rightarrow σ^* (C11-C16)	σ^* (C3-C4) \rightarrow σ^* (C1-C2)	236.54
FBDBT	σ^* (C14-C15) \rightarrow σ^* (C11-C16)	σ^* (C11-C16) \rightarrow σ^* (C27-H31)	1100.56
CIBDBT	σ^* (C3-C4) \rightarrow σ^* (C1-C2)	σ^* (C3-C4) \rightarrow σ^* (C1-C2)	228.32
BrBDBT	σ^* (C14-C15) \rightarrow σ^* (C11-C16)	σ^* (C22-C23) \rightarrow σ^* (C25-C29)	441.75
XA	σ^* (C4-C5) \rightarrow σ^* (C1-C6)	σ^* (C4-C5) \rightarrow σ^* (C1-C6)	191.23
AR	σ^* (C4-C5) \rightarrow σ^* (C1-C6)	σ^* (C4-C5) \rightarrow σ^* (C1-C6)	258.20
AD	σ^* (C8-C9) \rightarrow σ^* (C4-C7)	σ^* (C8-C9) \rightarrow σ^* (C4-C7)	191.85

The NBO analysis was helpful to find out the types and composition of various molecular orbitals, as well as for the intramolecular and intermolecular hyperconjugation interactions. The electron withdrawing group, electron donor group, and cyclohexene ring were the groups that often needed to be introduced in the synthesis of anthraquinone compounds. When different substituent groups were introduced, the excited states of different systems had different sensitivities when the structure changed. The order of electronic state energy levels of the anthraquinone compounds changed when compared with anthraquinone. The influence of these effects led to the rearrangement of the order of electronic state energy levels and thus affected the selection of the excited atoms for anthraquinone compounds.

Table 4 illustrates the charge transfer characteristics and the stabilization energies, E (2), of the AQs. The twelve compounds studied in this paper mainly exhibit the $\sigma^* \rightarrow \sigma^*$ transition form. For all the molecules except for the BDBTs (BDBT, CIBDBT, FBDBT, BrBDBT), the charge transfer characteristics and the stabilization energies were computed with the basis set of cc-pVTZ; furthermore, they were the same with the one obtained with the aug-cc-pVTZ basis set. In BDBTs, only CIBDBT has the same charge transfer

characteristics and stabilization energy for both the cc-pVTZ and aug-cc-pVTZ basis sets. For the other BDBTs, i.e., in the basis set of cc-pVTZ, the charge transfer characteristics of the BDBT, FBDBT, and BrBDBT were $\sigma^*(\text{C14-C15}) \rightarrow \sigma^*(\text{C11-C16})$, $\sigma^*(\text{C14-C15}) \rightarrow \sigma^*(\text{C11-C16})$, and $\sigma^*(\text{C14-C15}) \rightarrow \sigma^*(\text{C11-C16})$ —with stabilization energies of 516.26 kcal/mol, 307.23 kcal/mol, and 457.47 kcal/mol—respectively. In the aug-cc-pVTZ, charge transfer characteristics of the BDBT, FBDBT, and BrBDBT the values were $\sigma^*(\text{C3-C4}) \rightarrow \sigma^*(\text{C1-C2})$, $\sigma^*(\text{C11-C16}) \rightarrow \sigma^*(\text{C27-H31})$ and $\sigma^*(\text{C22-C23}) \rightarrow \sigma^*(\text{C25-C29})$ —with stabilization energies of 236.54 kcal/mol, 1100.56 kcal/mol, and 441.75 kcal/mol—respectively. Thus, in the BDBT's charge transfer characteristics and the stabilization energies were more sensitive to the basis set.

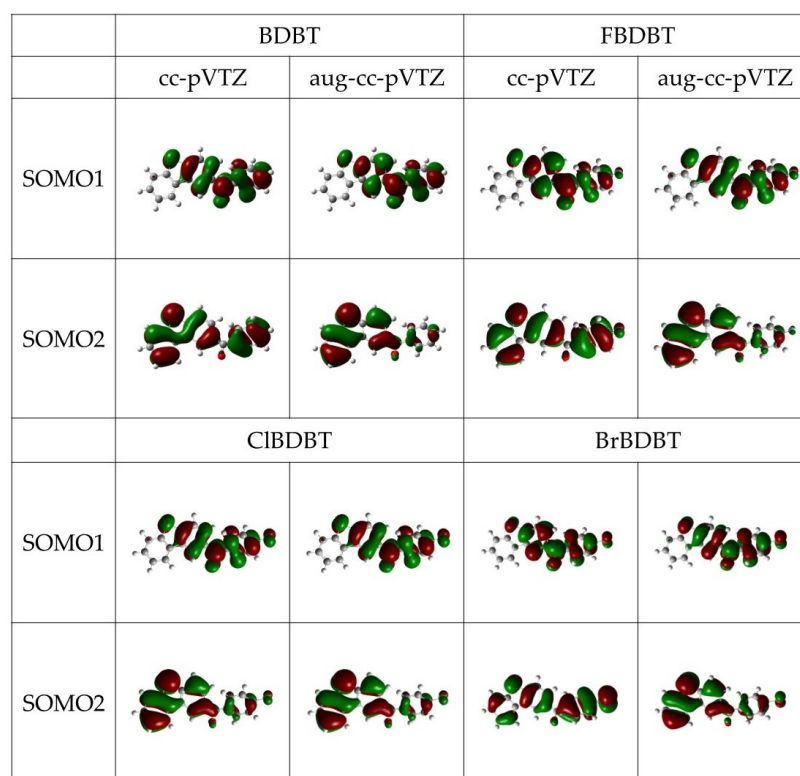


Figure 3. Molecular orbital diagrams of the SOMO1 and the SOMO2 that were obtained by choosing aug-cc-pVDZ and aug-cc-pVTZ for the BDBT, FBDBT, CIBDBT and BrBDBT calculations.

Here, we refer to the two singly occupied molecular orbitals (SOMOs) as SOMO1 and SOMO2. We could see that these SOMO orbitals exhibit strong charge separation properties when the diffuse function was added to the basis set. Additionally, when the basis set without the diffuse function was used, for the BDBT, FBDBT, BrBDBT, the charge separation was not as strong as it was for CIBDBT, and they were all on the same side. This is attributed to the fact that the conjugation of chlorine was better than the others, as bromine was too large, fluorine was too electronegative, and the BDBT had no substituent. This meant that the basis set with a diffuse function was very important, especially when using M06-HF. However, without the diffuse function in the basis set, the charge separation became smaller and the error increased.

4. Conclusions

In this work, phosphorescence energy was studied via TDDFT and UDFT with seven functionals (PEB, PBE0, B3LYP, CAM-B3LYP, ω B97XD, M06-2X, and M06-HF) and four basis sets (cc-pVDZ, cc-pVTZ, aug-cc-pVDZ, and aug-cc-pVTZ). TDDFT and UDFT were used to optimize the geometry and to calculate the phosphorescence energy, respectively. For the geometry optimization, the RMSD between the geometries optimized by TDDFT

and UDFT was about 0.03 Å, thereby indicating that the two geometries were very close. However, as the TDDFT suffered from a Rydberg state, which was not easy to converge, UDFT was more suitable for the geometry optimization. In the phosphorescence energy calculation, when using CC2 as a reference, the MUE of UDFT was 0.14 eV, which is smaller than the MUE of TDDFT which was at 0.29 eV. Therefore, UDFT is more suitable for the calculation of phosphorescence energy. For the functional effect, we found that with increasing the Hartree–Fock exchange, the MUE decreased from 0.66 eV to 0.18 eV. Interestingly, the M06-2X functional had the smallest MUE values of 0.14 eV, thus indicating that the M06 series of the functionals were more suitable for describing the phosphorescence energy. More importantly, the M06-HF functional was very sensitive to the basis set. In the BDBT, FBDBT, and BrBDBT molecules, by using the basis set without the diffuse function, the phosphorescence energy difference between the M06-HF and CC2 was above 0.80 eV. However, by adding the diffuse function to the basis set, this decreased to 0.02 eV. The results of the NBO analysis on the charge transfer characteristics and stabilization energies show that the BDBT, FBDBT, and BrBDBT were more sensitive to the diffuse function of the basis set. This work has systemically studied geometry optimization and phosphorescence energy with different functionals and basis sets by using the TDDFT and UDFT methods; these findings are of particular importance for the further study of the phosphorescence energy of other organics.

Supplementary Materials: The following supporting information can be downloaded at: <https://www.mdpi.com/article/10.3390/molecules28073257/s1>, Figure S1: The MUE values (excluding BDBT, FBDBT, CIBDBT, BrBDBT) obtained by different basis sets under the same phosphorescence energy calculation method and functionals. (a), (b), (c), and (d) represent the results obtained with the basis set of cc-pVDZ, cc-pVTZ, aug-cc-pVDZ, and aug-cc-pVTZ, respectively.; Tables S1–S13: Cartesian coordinates (Å) of optimized geometries. Table S2: The geometry optimization with TDDFT and UDFT for HA, AAT, BP, TX-BT, TX-DBT, BDBT, FBDBT, CIBDBT, BrBDBT, XA, AR and AD are singlet and triplet, respectively. ΔE_1 and ΔE_2 (in eV) are the energy difference between the first excited triplet states and the second excited triplet states obtained by TDDFT and the ground states. The ground states and excited states energy calculated by UDFT are E_s and E_t (in a.u.). Tables S14–S17: The energy differences ΔE (in eV) relative to experimental values for the phosphorescence energy of AQs (except for BDBT, FBDBT, BrBDBT) calculated by TD//TDDFT, TD//UDFT, U//UDFT and TD//UDFT with different functionals (PBE, PBE0, B3LYP, CAM-B3LYP, ω B97XD, M062X, M06HF) at the cc-pVTZ level. Tables S18 and S19: The energy differences ΔE (in eV) relative to CC2 for the phosphorescence energy of AQs calculated by U//TDDFT and TD//TDDFT with different functionals (PBE, PBE0, B3LYP, CAM-B3LYP, ω B97XD, M062X, M06HF) at the cc-pVTZ level. Table S20: The energy differences ΔE (in eV) relative to CC2 for the phosphorescence energy of AQs (except for BDBT, FBDBT, BrBDBT) calculated by U//UDFT with different functionals (PBE, PBE0, B3LYP, CAM-B3LYP, ω B97XD, M062X, M06HF) at the cc-pVTZ level. Table S21: In M06HF functional the BDBT, FBDBT, CIBDBT and BrBDBT, the phosphorescence energy calculated by cc-pVDZ, cc-pVTZ, aug-cc-pVDZ, aug-cc-pVTZ and CC2. Table S22: The S^2 values for the triplet states of AQs calculated by UDFT with different functionals (PBE, PBE0, B3LYP, CAM-B3LYP, ω B97XD, M062X, M06HF) at the cc-pVTZ level.

Author Contributions: Investigation, L.Z.; Writing — review & editing, Y.G.; Supervision, Z.Q. All authors have read and agreed to the published version of the manuscript.

Funding: This work was supported, in part, by the National Natural Science Foundation of China (No. 21873036).

Institutional Review Board Statement: Not applicable.

Informed Consent Statement: Not applicable.

Data Availability Statement: Not applicable.

Conflicts of Interest: The authors declare no conflict of interest.

References

1. Zhao, W.; He, Z.; Tang, B.Z. Room-temperature phosphorescence from organic aggregates. *Nat. Rev. Mater.* **2020**, *5*, 869–885. [[CrossRef](#)]
2. Jacquemin, D.; Wathelet, V.; Perpète, E.A.; Adamo, C. Extensive TD-DFT Benchmark: Singlet-Excited States of Organic Molecules. *J. Chem. Theory Comput.* **2009**, *5*, 2420–2435. [[CrossRef](#)]
3. Mukherjee, S.; Thilagar, P. Recent advances in purely organic phosphorescent materials. *Chem. Commun.* **2015**, *51*, 10988–11003. [[CrossRef](#)]
4. Li, Z.; Liu, W. Critical Assessment of Time-Dependent Density Functional Theory for Excited States of Open-Shell Systems: II. Doublet-Quartet Transitions. *J. Chem. Theory Comput.* **2016**, *12*, 2517–2527. [[CrossRef](#)] [[PubMed](#)]
5. Baryshnikov, G.; Minaev, B.; Agren, H. Theory and Calculation of the Phosphorescence Phenomenon. *Chem. Rev.* **2017**, *117*, 6500–6537. [[CrossRef](#)]
6. Niehaus, T.A.; Hofbeck, T.; Yersin, H. Charge-transfer excited states in phosphorescent organo-transition metal compounds: A difficult case for time dependent density functional theory? *RSC Adv.* **2015**, *5*, 63318–63329. [[CrossRef](#)]
7. De Souza, B.; Farias, G.; Neese, F.; Izsak, R. Predicting Phosphorescence Rates of Light Organic Molecules Using Time-Dependent Density Functional Theory and the Path Integral Approach to Dynamics. *J. Chem. Theory Comput.* **2019**, *15*, 1896–1904. [[CrossRef](#)] [[PubMed](#)]
8. Grotjahn, R.; Kaupp, M. Reliable TDDFT Protocol Based on a Local Hybrid Functional for the Prediction of Vibronic Phosphorescence Spectra Applied to Tris(2,2'-bipyridine)-Metal Complexes. *J. Phys. Chem. A* **2021**, *125*, 7099–7110. [[CrossRef](#)] [[PubMed](#)]
9. Shi, H.; An, Z.; Li, P.-Z.; Yin, J.; Xing, G.; He, T.; Chen, H.; Wang, J.; Sun, H.; Huang, W.; et al. Enhancing Organic Phosphorescence by Manipulating Heavy-Atom Interaction. *Cryst. Growth Des.* **2016**, *16*, 808–813. [[CrossRef](#)]
10. Kenry; Chen, C.; Liu, B. Enhancing the performance of pure organic room-temperature phosphorescent luminophores. *Nat. Commun.* **2019**, *10*, 2111. [[CrossRef](#)]
11. El-Sayed, M.A. Spin—Orbit Coupling and the Radiationless Processes in Nitrogen Heterocyclics. *J. Chem. Phys.* **1963**, *38*, 2834–2838. [[CrossRef](#)]
12. Zhang, H.; Guo, Y.; Wu, Z.; Wang, Y.; Sun, Y.; Feng, X.; Wang, H.; Zhao, G. Unveiling the theoretical mechanism of purely organic room temperature phosphorescence emission and heteroatomic effects on singlet-triplet intersystem crossing for isopropylthioxanthone derivatives. *J. Lumin.* **2021**, *232*, 117864. [[CrossRef](#)]
13. Jacquemin, D.; Assfeld, X.; Preat, J.; Perpète, E.A. Comparison of theoretical approaches for predicting the UV/Vis spectra of anthraquinones. *Mol. Phys.* **2007**, *105*, 325–331. [[CrossRef](#)]
14. Goudappagouda; Nidhankar, A.D.; Nayak, R.A.; Santhosh Babu, S. Aggregation-induced phosphorescence of an anthraquinone based emitter. *Org. Biomol. Chem.* **2021**, *19*, 1004–1008. [[CrossRef](#)] [[PubMed](#)]
15. Diaz, A.N. Absorption and Emission Spectroscopy and Photochemistry of 1,10-Anthraquinone Derivatives: A Review. *J. Photochem. Photobiol. A-Chem.* **1989**, *53*, 141–167. [[CrossRef](#)]
16. Schreiber, M.; Silva-Junior, M.R.; Sauer, S.P.; Thiel, W. Benchmarks for electronically excited states: CASPT2, CC2, CCSD, and CC3. *J. Chem. Phys.* **2008**, *128*, 134110. [[CrossRef](#)]
17. Sauer, S.P.; Schreiber, M.; Silva-Junior, M.R.; Thiel, W. Benchmarks for Electronically Excited States: A Comparison of Noniterative and Iterative Triples Corrections in Linear Response Coupled Cluster Methods: CCSDR(3) versus CC3. *J. Chem. Theory Comput.* **2009**, *5*, 555–564. [[CrossRef](#)]
18. Christiansen, O.; Koch, H.; Jørgensen, P. Response functions in the CC3 iterative triple excitation model. *J. Chem. Phys.* **1995**, *103*, 7429–7441. [[CrossRef](#)]
19. Christiansen, O.; Koch, H.; Jørgensen, P. Perturbative triple excitation corrections to coupled cluster singles and doubles excitation energies. *J. Chem. Phys.* **1996**, *105*, 1451–1459. [[CrossRef](#)]
20. Andersson, K.; Malmqvist, P.Å.; Roos, B.O. Second-order perturbation theory with a complete active space self-consistent field reference function. *J. Chem. Phys.* **1992**, *96*, 1218–1226. [[CrossRef](#)]
21. Andersson, K.; Malmqvist, P.A.; Roos, B.O.; Sadlej, A.J.; Wolinski, K. Second-Order Perturbation Theory with a CASSCF Reference Function. *J. Phys. Chem.* **1990**, *94*, 5483–5488. [[CrossRef](#)]
22. Christiansen, O.; Koch, H.; Jørgensen, P. The second-order approximate coupled cluster singles and doubles model CC2. *Chem. Phys. Lett.* **1995**, *243*, 409–418. [[CrossRef](#)]
23. Dominique Guillaumont, S.N. Calculation of the absorption wavelength of dyes using time-dependent density-functional theory (TD-DFT). *Dye. Pigment.* **2000**, *46*, 85–92. [[CrossRef](#)]
24. Serrano-Andrés, L.; Roos, B.O. A Theoretical Study of the Indigoid Dyes and Their Chromophore. *Clwm. Eztr. J.* **1997**, *3*, 717–725. [[CrossRef](#)]
25. Parac, M.; Grimme, S. Comparison of Multireference Møller-Plesset Theory and Time-Dependent Methods for the Calculation of Vertical Excitation Energies of Molecules. *J. Phys. Chem. A* **2002**, *106*, 6844–6850. [[CrossRef](#)]
26. Fabian, J.; Diaz, L.A.; Seifert, G.; Niehaus, T. Calculation of excitation energies of organic chromophores: A critical evaluation. *J. Mol. Struct.* **2002**, *594*, 41–53. [[CrossRef](#)]
27. Blancafort, L.; Robb, M.A. Key Role of a Threefold State Crossing in the Ultrafast Decay of Electronically Excited Cytosine. *J. Phys. Chem. A* **2004**, *108*, 10609–10614. [[CrossRef](#)]

28. Shemesh, D.; Sobolewski, A.L.; Domcke, W. Efficient Excited-State Deactivation of the Gly-Phe-Ala Tripeptide via an Electron-Driven Proton-Transfer Process. *J. Comput. Chem.* **2009**, *131*, 1374–1375. [[CrossRef](#)] [[PubMed](#)]
29. Blancafort, L.; Voityuk, A.A. MS-CASPT2 Calculation of Excess Electron Transfer in Stacked DNA Nucleobases. *J. Phys. Chem. A* **2007**, *111*, 4714–4719. [[CrossRef](#)] [[PubMed](#)]
30. Kohn, W.; Sham, L.J. Self-Consistent Equations Including Exchange and Correlation Effects. *Phys. Rev.* **1965**, *140*, A1133–A1138. [[CrossRef](#)]
31. Goerigk, L.; Hansen, A.; Bauer, C.; Ehrlich, S.; Najibi, A.; Grimme, S. A look at the density functional theory zoo with the advanced GMTKN55 database for general main group thermochemistry, kinetics and noncovalent interactions. *Phys. Chem. Chem. Phys.* **2017**, *19*, 32184–32215. [[CrossRef](#)]
32. Mardirossian, N.; Head-Gordon, M. Thirty years of density functional theory in computational chemistry: An overview and extensive assessment of 200 density functionals. *Mol. Phys.* **2017**, *115*, 2315–2372. [[CrossRef](#)]
33. Stratmann, R.E.; Scuseria, G.E.; Frisch, M.J. An efficient implementation of time-dependent density-functional theory for the calculation of excitation energies of large molecules. *J. Chem. Phys.* **1998**, *109*, 8218–8224. [[CrossRef](#)]
34. Petersilka, M.G.U.J.; Gossmann, U.J.; Gross, E.K.U. Excitation Energies from Time-Dependent Density-Functional Theory. *Phys. Rev. Lett.* **1996**, *76*, 1212–1214. [[CrossRef](#)] [[PubMed](#)]
35. Runge, E.; Gross, E.K.U. Density-Functional Theory for Time-Dependent Systems. *Phys. Rev. Lett.* **1984**, *52*, 997–1000. [[CrossRef](#)]
36. Andreas Dreuw, M.H.-G. Single-Reference ab Initio Methods for the Calculation of Excited States of Large Molecules. *Chem. Rev.* **2005**, *105*, 4009–4037. [[CrossRef](#)]
37. Perdew, J.P.; Ruzsinszky, A.; Tao, J.; Staroverov, V.N.; Scuseria, G.E.; Csonka, G.I. Prescription for the design and selection of density functional approximations: More constraint satisfaction with fewer fits. *J. Chem. Phys.* **2005**, *123*, 62201. [[CrossRef](#)] [[PubMed](#)]
38. Fetter, A.L.; Walecka, J.D. *Quantum Theory of Many-Particle Systems*; Courier Corporation: North Chelmsford, MA, USA, 2012.
39. Hirata, S.; Lee, T.J.; Head-Gordon, M. Time-dependent density functional study on the electronic excitation energies of polycyclic aromatic hydrocarbon radical cations of naphthalene, anthracene, pyrene, and perylene. *J. Chem. Phys.* **1999**, *111*, 8904–8912. [[CrossRef](#)]
40. Hirata, S.; Head-Gordon, M. Time-dependent density functional theory within the Tamm–Dancoff approximation. *Chem. Phys. Lett.* **1999**, *314*, 291–299. [[CrossRef](#)]
41. Handy, N.C.; Tozer, D.J. Excitation Energies of Benzene from Kohn–Sham Theory. *J. Comput. Chem.* **1998**, *20*, 106–113. [[CrossRef](#)]
42. Peach, M.J.; Benfield, P.; Helgaker, T.; Tozer, D.J. Excitation energies in density functional theory: An evaluation and a diagnostic test. *J. Chem. Phys.* **2008**, *128*, 044118. [[CrossRef](#)] [[PubMed](#)]
43. Isegawa, M.; Peverati, R.; Truhlar, D.G. Performance of recent and high-performance approximate density functionals for time-dependent density functional theory calculations of valence and Rydberg electronic transition energies. *J. Chem. Phys.* **2012**, *137*, 244104. [[CrossRef](#)] [[PubMed](#)]
44. Peverati, R.; Truhlar, D.G. Performance of the M11 and M11-L density functionals for calculations of electronic excitation energies by adiabatic time-dependent density functional theory. *Phys. Chem. Chem. Phys.* **2012**, *14*, 11363–11370. [[CrossRef](#)] [[PubMed](#)]
45. Jacquemin, D.; Perpète, E.A.; Ciofini, I.; Adamo, C.; Valero, R.; Zhao, Y.; Truhlar, D.G. On the Performances of the M06 Family of Density Functionals for Electronic Excitation Energies. *J. Chem. Theory Comput.* **2010**, *6*, 2071–2085. [[CrossRef](#)] [[PubMed](#)]
46. Schira, R.; Latouche, C. DFT vs. TDDFT vs. TDA to simulate phosphorescence spectra of Pt- and Ir-based complexes. *Dalton Trans.* **2021**, *50*, 746–753. [[CrossRef](#)] [[PubMed](#)]
47. Nakatsuji, H. Cluster Expansion of the Wavefunction-Excited States. *Chem. Phys. Lett.* **1978**, *59*, 362–364. [[CrossRef](#)]
48. Bousquet, D.; Fukuda, R.; Jacquemin, D.; Ciofini, I.; Adamo, C.; Ehara, M. Benchmark Study on the Triplet Excited-State Geometries and Phosphorescence Energies of Heterocyclic Compounds: Comparison Between TD-PBE0 and SAC-CI. *J. Chem. Theory Comput.* **2014**, *10*, 3969–3979. [[CrossRef](#)]
49. Khalid, M.; Hussain, R.; Hussain, A.; Ali, B.; Jaleel, F.; Imran, M.; Assiri, M.A.; Usman Khan, M.; Ahmed, S.; Abid, S.; et al. Electron Donor and Acceptor Influence on the Nonlinear Optical Response of Diacetylene-Functionalized Organic Materials (DFOMs): Density Functional Theory Calculations. *Molecules* **2019**, *24*, 2096. [[CrossRef](#)]
50. Haroon, M.; Khalid, M.; Akhtar, T.; Tahir, M.N.; Khan, M.U.; Muhammad, S.; Al-Sehemi, A.G.; Hameed, S. Synthesis, crystal structure, spectroscopic, electronic and nonlinear optical properties of potent thiazole based derivatives: Joint experimental and computational insight. *J. Mol. Struct.* **2020**, *1202*, 127354. [[CrossRef](#)]
51. Khalid, M.; Naseer, S.; Tahir, M.S.; Shafiq, I.; Munawar, K.S.; de Alcântara Morais, S.F.; Braga, A.A. A theoretical approach towards designing of banana shaped non-fullerene chromophores using efficient acceptors moieties: Exploration of their NLO response properties. *Opt. Quantum Electron.* **2023**, *55*, 258. [[CrossRef](#)]
52. Baek, Y.S.; Lee, S.; Filatov, M.; Choi, C.H. Optimization of Three State Conical Intersections by Adaptive Penalty Function Algorithm in Connection with the Mixed-Reference Spin-Flip Time-Dependent Density Functional Theory Method (MRSF-TDDFT). *J. Phys. Chem. A* **2021**, *125*, 1994–2006. [[CrossRef](#)]
53. Yu, H.S.; Li, S.L.; Truhlar, D.G. Perspective: Kohn–Sham density functional theory descending a staircase. *J. Chem. Phys.* **2016**, *145*, 130901. [[CrossRef](#)] [[PubMed](#)]
54. Gräfenstein, J.; Kraka, E.; Filatov, M.; Cremer, D. Can Unrestricted Density-Functional Theory Describe Open Shell Singlet Biradicals? *Int. J. Mol. Sci.* **2002**, *3*, 360–394. [[CrossRef](#)]

55. Gräfenstein, J.; Hjerpe, A.M.; Kraka, E.; Cremer, D. An accurate description of the Bergman reaction using restricted and unrestricted DFT: Stability test, spin density, and on-top pair density. *J. Phys. Chem. A* **2000**, *104*, 1748–1761. [[CrossRef](#)]
56. Richtol, H.H.; Fitch, B.R. Triplet State Acidity Constants for Hydroxy and Amino Substituted Anthraquinones and Related Compounds. *Anal. Chem.* **1974**, *46*, 1860–1862. [[CrossRef](#)]
57. Bayrakceken, F. Triplet-triplet optical energy transfer from benzophenone to naphthalene in the vapor phase. *Spectrochim. Acta Part A-Mol. Biomol. Spectrosc.* **2008**, *71*, 603–608. [[CrossRef](#)]
58. Karaca, N.; Ocal, N.; Arsu, N.; Jockusch, S. Thioxanthone-benzothiophenes as photoinitiator for free radical polymerization. *J. Photochem. Photobiol. A-Chem.* **2016**, *331*, 22–28. [[CrossRef](#)]
59. He, Z.; Zhao, W.; Lam, J.W.Y.; Peng, Q.; Ma, H.; Liang, G.; Shuai, Z.; Tang, B.Z. White light emission from a single organic molecule with dual phosphorescence at room temperature. *Nat. Commun.* **2017**, *8*, 416. [[CrossRef](#)]
60. McMorro, D.; Wyche, M.I.; Chou, P.T.; Kasha, M. On the dual phosphorescence of xanthone and chromone in glassy hydrocarbon hosts. *Photochem. Photobiol.* **2015**, *91*, 576–585. [[CrossRef](#)]
61. De Silva, J.A.F.; Strojny, N.; Stika, K. Luminescence determination of pharmaceuticals of the tetrahydrocarbazole, carbazole, and 1, 4-benzodiazepine class. *Anal. Chem.* **1976**, *48*, 144–155. [[CrossRef](#)]
62. Dansholm, C.N.; Junker, A.K.R.; Nielsen, L.G.; Kofod, N.; Pal, R.; Sorensen, T.J. pi-Expanded Thioxanthenes—Engineering the Triplet Level of Thioxanthone Sensitizers for Lanthanide-Based Luminescent Probes with Visible Excitation. *Chempluschem* **2019**, *84*, 1778–1788. [[CrossRef](#)]
63. Shukla, D.; Ahearn, W.G.; Farid, S. Chain Amplification in Photoreactions of N-Alkoxy pyridinium Salts with Alcohols: Mechanism and Kinetics. *J. Org. Chem.* **2005**, *70*, 6809–6819. [[CrossRef](#)] [[PubMed](#)]
64. Adamo, C.; Barone, V. Toward reliable density functional methods without adjustable parameters: The PBE0 model. *J. Chem. Phys.* **1999**, *110*, 6158–6169. [[CrossRef](#)]
65. Reiher, M.; Salomon, O.; Artur Hess, B. Reparameterization of hybrid functionals based on energy differences of states of different multiplicity. *Theor. Chem. Acc.* **2001**, *107*, 48–55. [[CrossRef](#)]
66. Yanai, T.; Tew, D.P.; Handy, N.C. A new hybrid exchange–correlation functional using the Coulomb-attenuating method (CAM-B3LYP). *Chem. Phys. Lett.* **2004**, *393*, 51–57. [[CrossRef](#)]
67. Chai, J.D.; Head-Gordon, M. Long-range corrected hybrid density functionals with damped atom-atom dispersion corrections. *Phys. Chem. Chem. Phys.* **2008**, *10*, 6615–6620. [[CrossRef](#)] [[PubMed](#)]
68. Zhao, Y.; Truhlar, D.G. The M06 suite of density functionals for main group thermochemistry, thermochemical kinetics, noncovalent interactions, excited states, and transition elements: Two new functionals and systematic testing of four M06-class functionals and 12 other functionals. *Theor. Chem. Acc.* **2007**, *120*, 215–241.
69. Zhao, Y.; Truhlar, D.G. Comparative DFT Study of van der Waals Complexes: Rare-Gas Dimers, Alkaline-Earth Dimers, Zinc Dimer, and Zinc-Rare-Gas Dimers. *J. Phys. Chem. A* **2006**, *110*, 5121–5129. [[CrossRef](#)]
70. Zhao, Y.; Truhlar, D.G. Density Functional for Spectroscopy: No Long-Range Self-Interaction Error, Good Performance for Rydberg and Charge-Transfer States, and Better Performance on Average than B3LYP for Ground States. *J. Phys. Chem. A* **2006**, *110*, 13126–13130. [[CrossRef](#)]
71. Frisch, M.J.; Trucks, G.W.; Schlegel, H.B.; Scuseria, G.E.; Robb, M.A.; Cheeseman, J.R.; Scalmani, G.; Barone, V.; Petersson, G.A.; Nakatsuji, H.; et al. *Gaussian 16 Rev. C.01*; Gaussian Inc.: Wallingford, CT, USA, 2016.
72. Werner, H.-J.; Knowles, P.J.; Knizia, G.; Manby, F.R.; Schütz, M. Molpro: A general-purpose quantum chemistry program package. *WIREs Comput. Mol. Sci.* **2012**, *2*, 242–253. [[CrossRef](#)]
73. Werner, H.J.; Knowles, P.J.; Manby, F.R.; Black, J.A.; Doll, K.; Hesselmann, A.; Kats, D.; Kohn, A.; Korona, T.; Kreplin, D.A.; et al. The Molpro quantum chemistry package. *J. Chem. Phys.* **2020**, *152*, 144107. [[CrossRef](#)] [[PubMed](#)]
74. Humphrey, W.; Dalke, A.; Schulten, K. VMD: Visual Molecular Dynamics. *J. Mol. Graph.* **1996**, *14*, 33–38. [[CrossRef](#)] [[PubMed](#)]

Disclaimer/Publisher’s Note: The statements, opinions and data contained in all publications are solely those of the individual author(s) and contributor(s) and not of MDPI and/or the editor(s). MDPI and/or the editor(s) disclaim responsibility for any injury to people or property resulting from any ideas, methods, instructions or products referred to in the content.